Characterizing the 410-km Discontinuity Low-Velocity Layer Beneath the LA RISTRA Array in the American Southwest

John Jasbinsek*, Ken Dueker, Steven Hansen and Zhu Zhang

Department of Geology & Geophysics, University of Wyoming

* Now at Department of Physics, California State Polytechnic University San Luis Obispo

Abstract

The water filter model predicts that the hydrous peridotite solidus may be crossed due to upflow of transition zone mantle containing >0.6-1% water by mass (Bercovici and Karato, 2003). For modest melt water contents, this hydrous melt is predicted to be denser than the upper mantle, but lighter than the transition zone; hence, the hydrous melt is predicted to perch upon the 410 km density contrast to form a gravitationally stable melt layer. If the water content of the melt exceeds 7%, then the melt is predicted to be positively buoyant with respect to the upper mantle, and upwards flow of melt rich diapirs is plausible (Inoue, 2007).

Recent seismic Pds analysis from dense western US PASSCAL arrays has found a mean 32 km thick low velocity layer atop the 410 km discontinuity with a 5-6% shear wave velocity reduction (Jasbinsek and Dueker, 2007; Jasbinsek et al., in review). These authors are unaware of an estimated melt-velocity scaling for the predicted 410 melt layer, but an upper mantle melt-velocity scaling of 1% melt causing a 2.2% shear reduction (Kreutzmann et al., 2004) may be close. Thus, the observed 410-LVL velocity reduction would require 2-3% melt porosities.

The figure immediately below shows the receiver function results for the LA RISTRA array grouped by backazimuth direction. A negative polarity arrival of equal of greater magnitude is consistently seen atop the 410 arrival. Remarkable is that the SE abnd SW back-azimuth receiver function traces find an absence of the 410-LVL signal at the SE end of the array (Texas/NM boarder). Beneath this region, an S-tomogram [Sine et al., 2008] shows a high velocity "blob" in the transition zone at 530 km depth (Section 5). This high velocity blob has been suggested to manifest a dripping-off of the lower lithospheric isotherms at the Texas/NM boarder (200 km il label) (Wilson et al., 2005). If this scenario is true, then the blob would have passed through the 410 km discontinuity. This flow scenario could thus provide an explanation for the absence of a 410-LVL beneath the Texas/NM boarder.

The arrows marked (1) and (2) in the same tomogram denote the possible that the low velocity melt-volumes, or blobs, above the 410 km discontinuity may manifest diapirs shed upwards from the 410 km melt layer. The 1-arrows mark where the low velocity blobs extend upwards from the 410 km discontinuity to the 10 Ma Jemez and 32 Ma Four Corners volcanic fields. Beneath the Texas/NM border, the 2-arrows speculate that the melt layer was destabilized by the transit of a sinking blob of destabilized lithosphere. The low velocity blob at 550 km depth (3-label) may relate to the water solubility contrast between wadsleyite and ringwoodite.

To isolate the P, SV and SH scattering response to incident teleseismic P-waves the Extended-Time Multi-Taper cross correlation technique is used [Helffrich 2006]. This method reduces spectral leakage in the frequency domain deconvolution. The large number of receiver functions in each trace provide excellent error estimation of the mean, allowing for reliable modeling of the 410-LVL.

1. Receiver Function Results

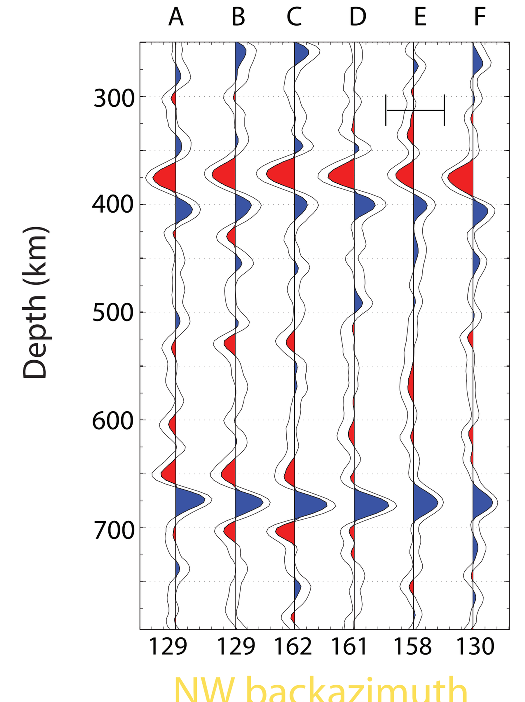

NW backazimuth

Map of LA RISTRA Array stations (below) and sampled regions at the 410 (yellow, red and blue contours). Data is divided into 6 partially overlapping regions (~190 km long) according to the backazimuth (NW, SE and SW) of the earthquake source. This provides 6 bins per backazimuth of receiver function data (labeled A-F) for a total of 18 bins. A total of 1951 receiver functions are used.

Receiver functions (RF) are migrated to depth using the Western US Tectonic Shear Wave model [Grand and Helmberger 1981] with Vp/Vs = 1.76 in the crust and 1.81 in the mantle.

In each bin individual RF are correlated with the mean of all RF in the bin, with correlations < 0.2 discarded. The resulting number of RF is labeled at the bottom of each of the three RF plots. The actual plots are the standard error bars of the mean RF determined from a bootstrapping procdeure. These plots are called ***quadrant stacks***.

Amplitude of the plotted quadrant stacks are relative to the vertical impulse response, with the black bar indicating +/- 5% relative amplitude to the impulse response.

In 14 of the 18 bins, a negative polarity arrival interferes with the 410 arrival with magnitude equal to or greater than the 410. We term this region of evidently low velocity atop the 410 layer the *410 Low-Velocity Layer or 410-LVL*. In this study we focus on modeling the 410-LVL, in particular its thickness and velocity reduction. Secondly, we speculate on the connection between our results and recent tomographic studies with the LA RISTRA data.

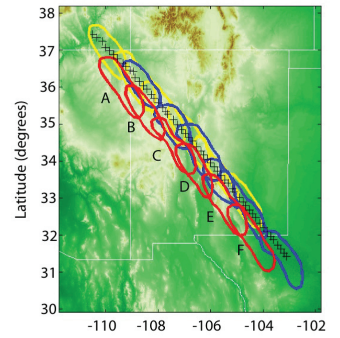

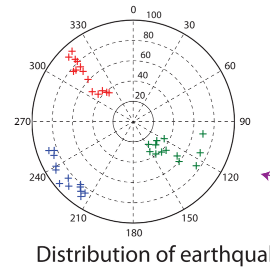

Distribution of earthquakes used in this study sorted by backazimuth (degrees) and distance (degrees) from the LA RISTRA array

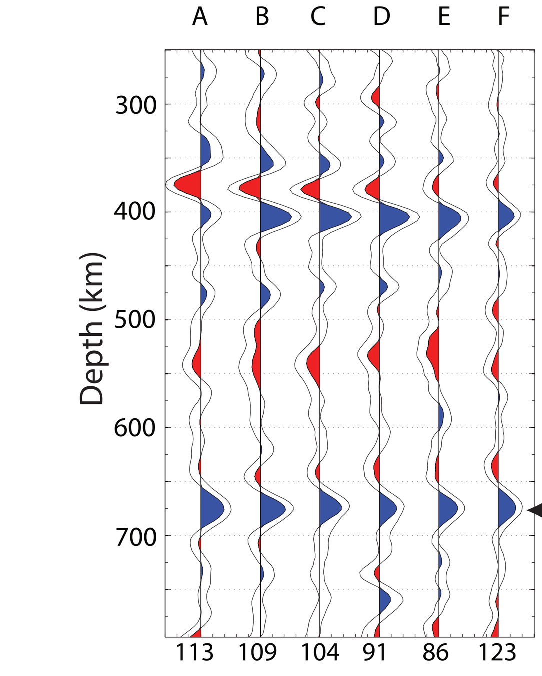

SW backazimuth

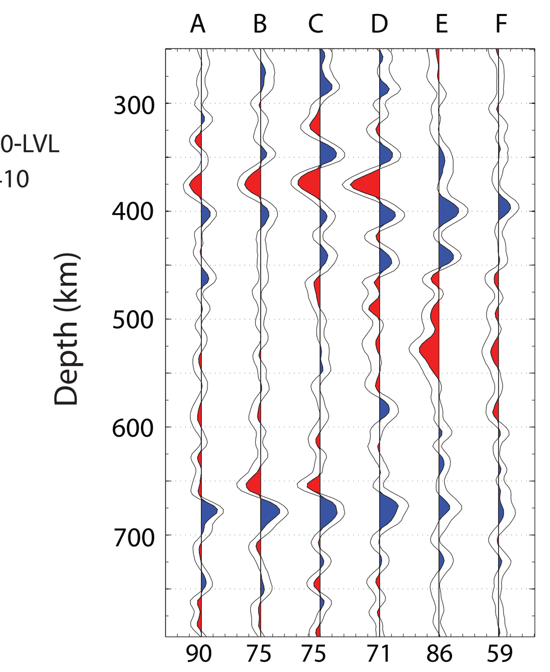

SE backazimuth

2. Modeling the 410-LVL: Double Gradient Slab (DGS) Velocity Models

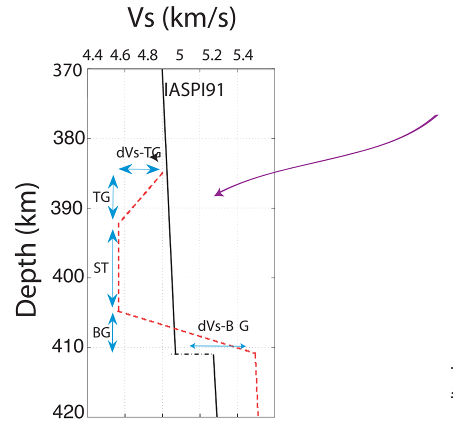

A five parameter velocity model perturbation to IASPI91 is used to calculate synthetic receiver functions: a top gradient thickness TG (km) and shear wave velocity reduction dVs-TG (km/s); a constant velocity slab layer thickness ST (km); and bottom gradient thickness BG (km) and shear velocity increase dVs-BG (km/s). Note that the bottom gradient thickness velocity increase defines the depth the IASPI91 velocity reduction is regained. This velocity model is termed the Double Gradient Slab model, or DGS (red dashed line). The linear velocity gradients in the DGS model are the simplest model capable of reproducing the negativity polarity P-S converted arrival interfering with the P410s arrival (see above).

A total of 116,160 synthetic receiver functions are calculated via a reflectivity code (Park 1996). Convolution with the estimated mean impulse response facilitates direct comparison with the observed data. Parameter value ranges and increments are shown in Table 1. The Futterman operator is applied to the synthetic receiver functions to account for anelastic effects.

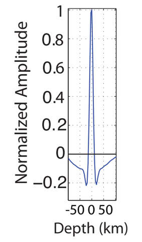

Estimated mean impulse response function convolved with the synthetic reflectivity series. The 20% side-lobes are accounted for in the modeling by the convolution with the synthetic reflectivity data.

Table 1. Parameter values of the double-gradient slab models.

Parameter	Minimum	Increment	Maximum
TG	0 (km)	5 (km)	45 (km)
BG	0 (km)	5 (km)	55 (km)
ST	0 (km)	5 (km)	35 (km)
dVs-TG	-0.90 (km/s)	0.06 (km/s)	0 (km/s)
dVs-BG	0 (km/s)	0.17 (km/s)	1.7 (km/s)

3. Modeling Results

The Global Waveform Stack

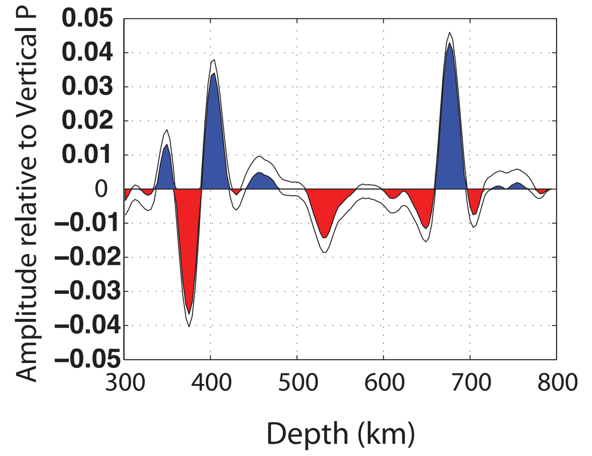

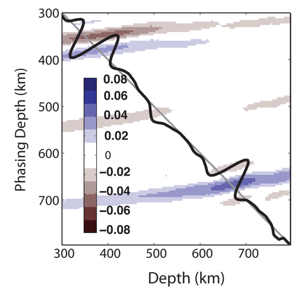

The Global Waveform Stack (GWS, left) is the linear stack of all 1951 receiver functions seen in Section 1. A clear 410-LVL, P410s and P660s which display the correct moveout (above) are seen. In addition, a negative polarity arrival with correct P-s moveout is seen at 530 km depth.

Modeling the Global Waveform Stack

Computation of DGS model likelihood: The probability of a velocity model *m* given receiver function data *d* is computed by a Gaussian likelihood function:

$$P(m\,|\,d) = \exp\left(-\frac{1}{2}(d-g(m))^T C_D^{-1}(d-g(m))\right)$$

where C_D is the data covariance matirx [Sambridge 1999].

Computation of the 1- and 2-D marginal probability distributions from the 5-D model probability volume are given by:

$$M_1(m_i) = \int\ldots\int P(m)\prod_{\substack{k=1\\k\neq i}}^{d} dm_k$$

$$M_2(m_i,m_j) = \int\ldots\int P(m)\prod_{\substack{k=1\\k\neq i,j}}^{d} dm_k$$

(where d is the number of model parameters, 5)
Alignment of model and data is achieved by minizing the L2 norm, thus the modeling only matches waveshape and not timing of the converted arrivals.

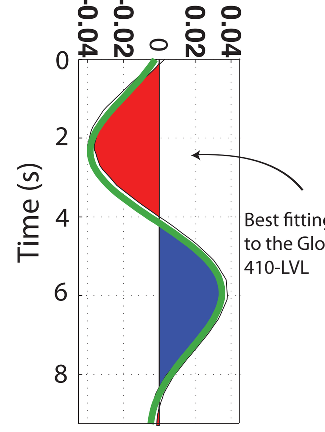

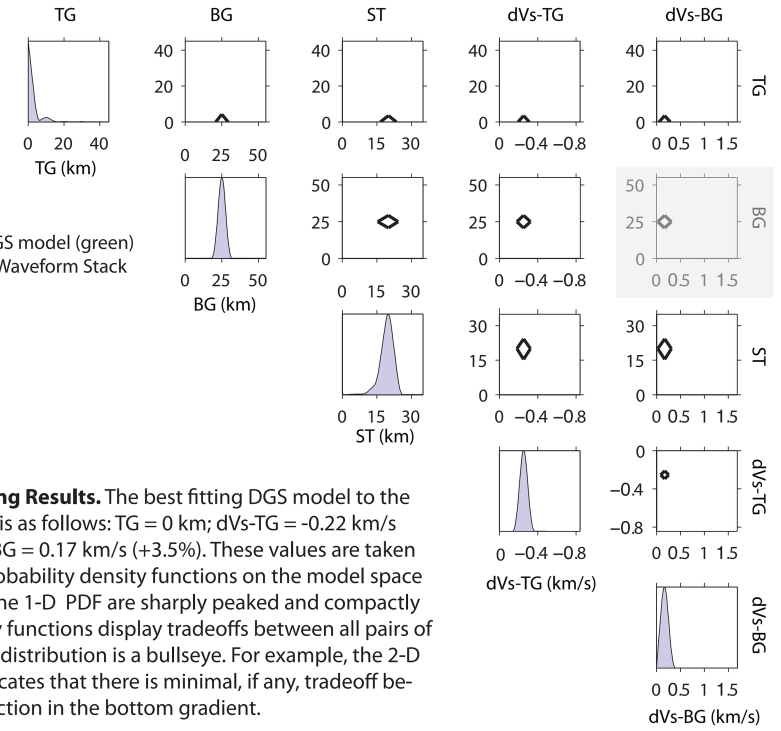

Global Waveform Stack DGS Modeling Results. The best fitting DGS model to the 410-LVL in the Global Waveform Stack is as follows: TG = 0 km; dVs-TG = -0.22 km/s (-4.6%); ST = 20 km; BG = 25 km; dVs-BG = 0.17 km/s (+3.5%). These values are taken from the peaks of the 1-D posterior probability density functions on the model space (above right, main diagonal). Each of the 1-D PDF are sharply peaked and compactly supported. The 2-D probability density functions display tradeoffs between all pairs of model parameters. In all cases the 2-D distribution is a bullseye. For example, the 2-D distribution lightly shaded in grey indicates that there is minimal, if any, tradeoff between the thickness and velocity reduction in the bottom gradient.

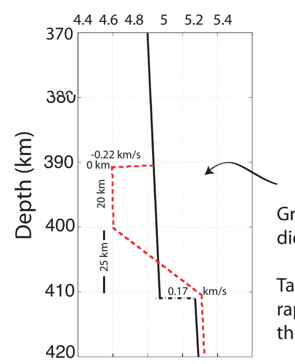

Graphic representation of the best fitting DGS model (red dashed line) to the Global Waveform Stack. The top gradient is sharp whereas the bottom gradient is diffuse. A 20-km thick constant velocity layer (ST) connects the top and bottom velocity gradients.

Taking half of each gradient width plus the constant velocity interval the 410-LVL is estimated to be 32.5 km thick. The sharp top gradient may indicate rapid quenching of the melt layer whereas the broad bottom gradient is consistent with a hydrated olivine-wadsleyite phase transformation. However, the boundary between the melt layer and olivine-wadsleyite phase transfomation in the BG is unknown.

4. Global Waveform Stack as a Mean to the 410-LVL Along the LA RISTRA Array

To demonstrate the Global Waveform Stack is a reasonable measure of the 410-LVL beneath the LA RISTRA Array, the best fitting DGS velocity model (black line) is plotted against each of the NW backazimuth quadrant stacks in Figure (A) below. This model by itself clearly provides a reasonable fit along the six different observed 410-LVL responses.

Figure (B) shows the results of applying the DGS models to each of the six NW backazimuth quadrant stacks. The best fitting DGS model is plotted on each quadrant stack with the reduced chi-square values labeled next to each waveform. The DGS models are clearly able to capture the differing waveshapes accurately. However, the simple linear velocity gradients can not capture more subtle curvature (2nd order) features of the velocity response in the 410-LVL.

Figure (C) shows the 1-D posterior probability distributions for each model parameter of each of the six (A-F) NW quadrant stacks. Evidently the distributions and their peaks overlap substantially, with a few exceptions, indicating that observed 410-LVL structure variations across the array are reasonably distributed about the mean structure (GWS).

(A)

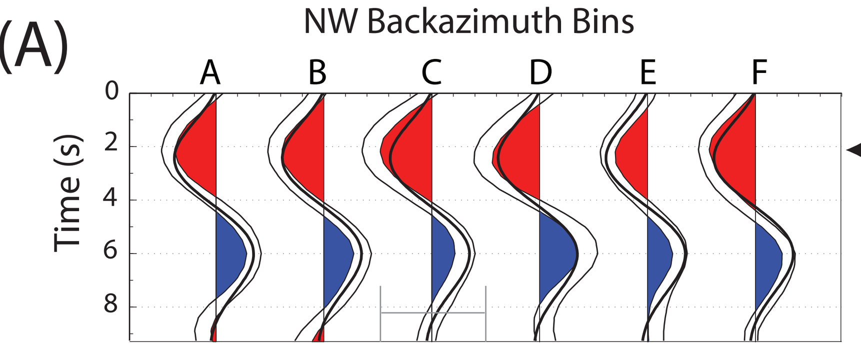

Best fitting DGS model to the Global Waveform Stack plotted against each NW backazimuth quadrant stack. Grey scale bar represents +/- 5% amplitude relative to vertical P.

(B)

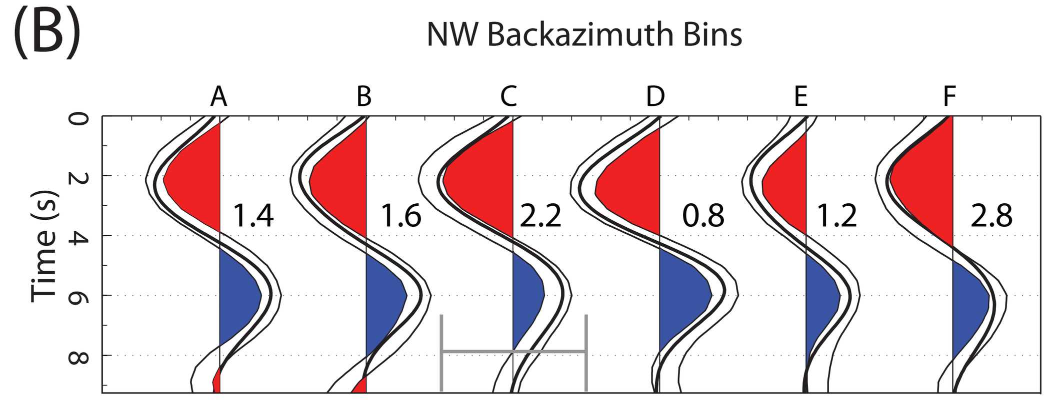

Best fitting DGS model for each NW quadrant stack anf associated chi-square value. Grey scale bar represents +/- 5% amplitude relative to vertical P.

(C)

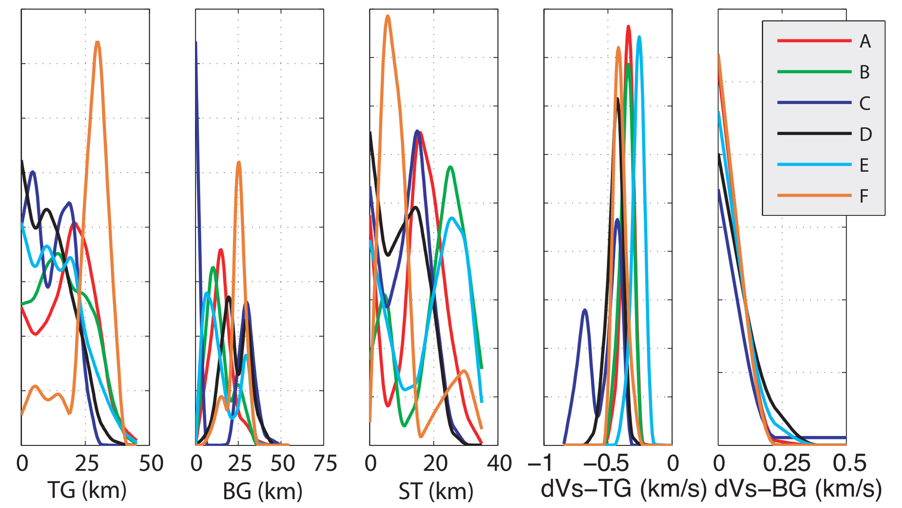

1-D posterior probability density functions for each DGS model parameter and NW quadrant bin. The six distributions for each model parameter substantially overlap, with a few exceptions.

5. Interpretation

1. The 410-LVL is interpreted as a manifestation of the Transition Zone Water Filter Model (Bercovici & Karato 2003). Other possible interpretations of the 410-LVL such as anisotropy are ruled out because tangential receiver functions are very low-energy. In addition, existence of a chemical anomaly atop the 410 is not supported by recent North American surface wave tomography (Bedle 2007, Earthscope conference).

Tangential Receiver Functions

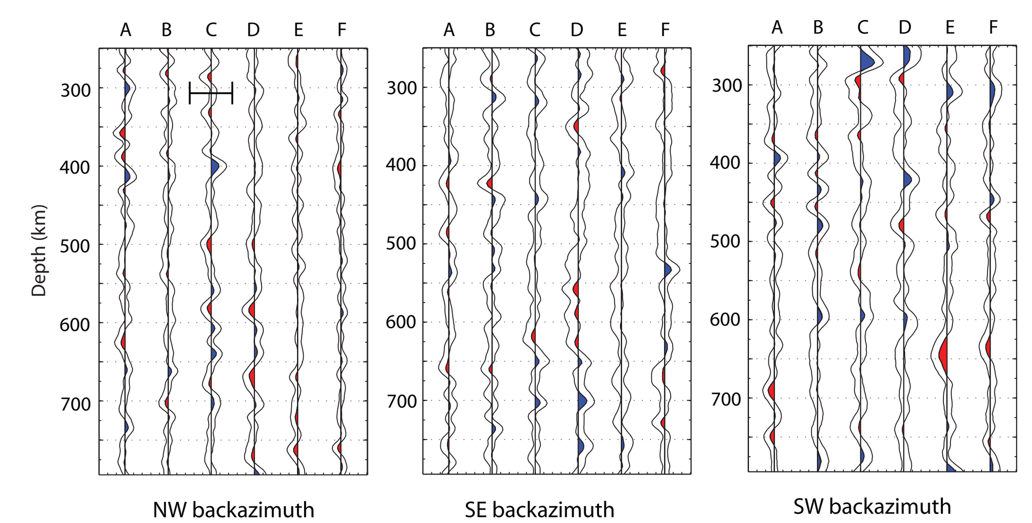

Tangential receiver functions. Grey scale bar represents +/- 5% amplitude relative to vertical P. The low energy tangential receiver functions rule out anispotropy as a primary component of the 410-LVL signal.

2. CCP stack of all 1951 receiver functions in this study clearly showing the 410, 660 and 410-LVL. Also present is an intermittent negative polarity arrival at 530 km depth. As in the receiver function quadrant stacks the 410-LVL is not present in the SE portion of the array. This is consistent with an interpretation of lithospheric delamination in this region by previous authors [Song & Helmberger 2007]. Foundering of lithospheric material into the upper transition zone region would mask the 410-LVL by quenching and/or advection of the 410-LVL material.
The negative polarity 530 arrival may be another aspect of the water-filter model. Beneath the 520-km (positive polarity) discontinuity ringwoodite is able to incorporate less water into its structure than the overlying wadsleyite. If local convection patterns bring sufficiently hydrated wadsleyite into the ringwoodite phase, local exsolution of water may occur causing a region of low seismic velocity. However, such a layer is unlikely to be static (as the 410-LVL) because there is no density contrast for the local melt to perch upon.

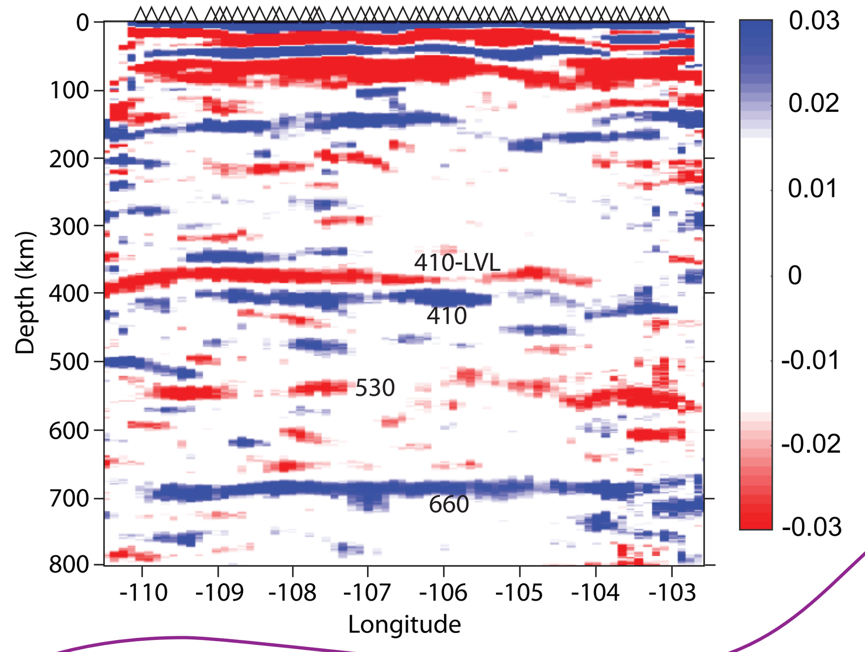

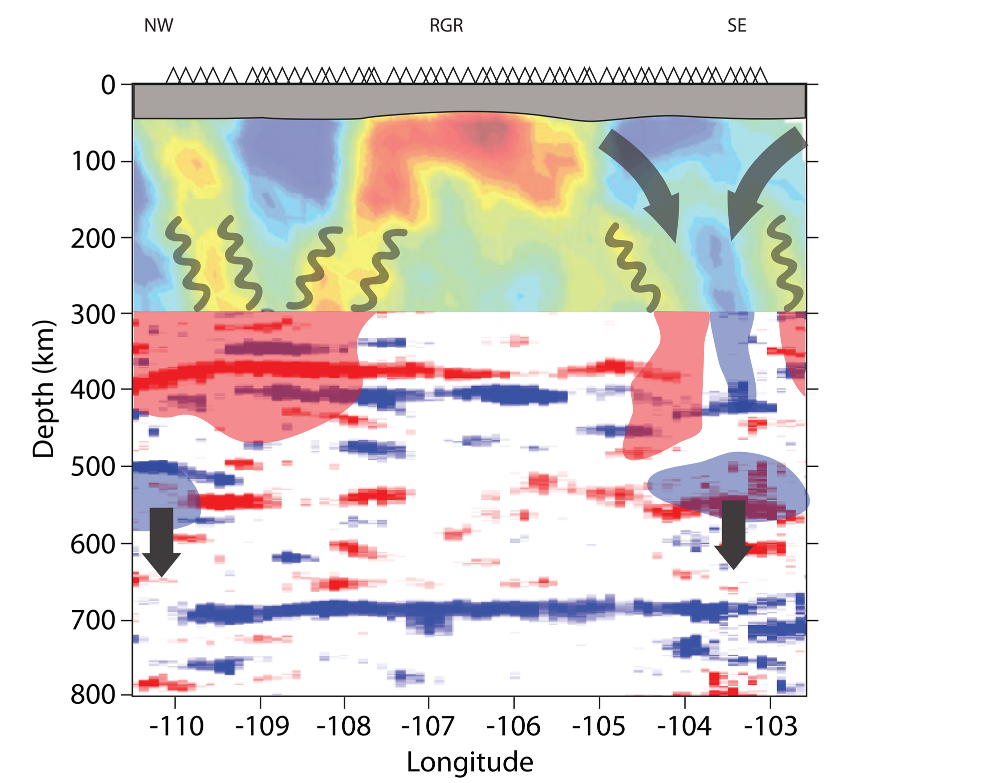

4. Interpretive figure of 410-LVL correlation with low-velocity anomalies in the upper mantle beneath the LA RISTRA Array. The CCP stack from this study is combined with the tomogram of Wilson & Aster 2005. The crust is denoted by the grey shaded region. Downward convective flow (large arrows) from lithospheric delamination mask the 410-LVL in the SE portion of the array. Upflow of hydrous melt-diapirs in the 410-LVL (squiggles) generate low-velocity anomalies in the upper mantle.

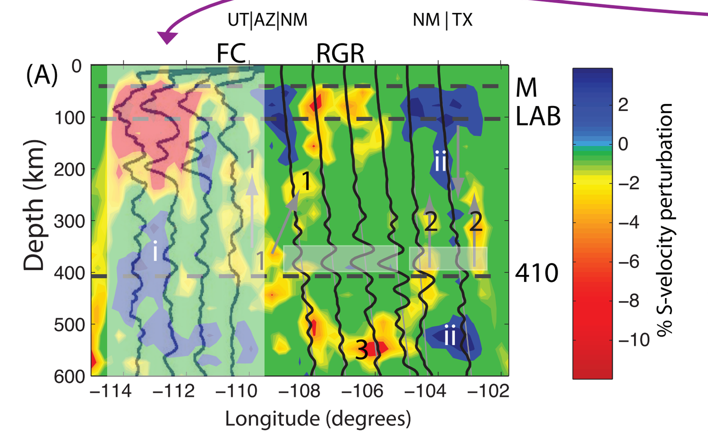

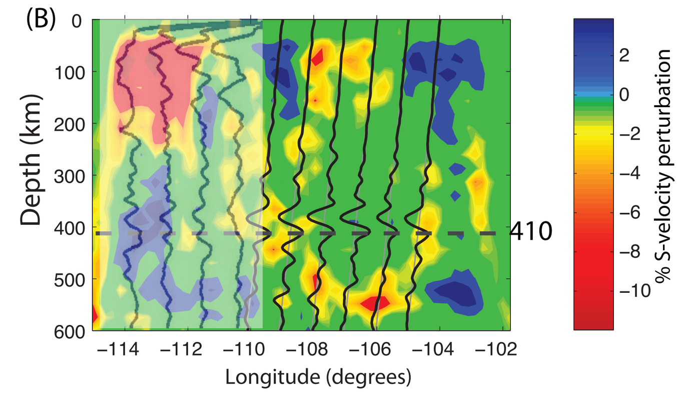

Shaded grey regions indicate the 410-LVL as delineated by the receiver function data. Receiver functions are oriented such that positive polarity is to the right. FC = Four Corners Region; RGR = Rio Grande Rift.

3. Overlay of NW and SE quadrant stacks on the S-tomogram of Sine et al., 2008. Low velocity anomalies in the upper mantle (labeled '1' and '2') may source from the 410-LVL. If the 410-LVL contains > 7% water the melt layer is predicted to be buoyant with respect to the base of the upper mantle (Inoue 2007). In this case a Rayleigh-Taylor like instability (rising diapir) may occur.
Under the assumption of a 10% denisty contrast to the surrounding mantle and a simple Stokes flow, the rising melt-volumes will impact the base of the lithosphere on the order of 10 million years.
The estimated S-velocity reduction (4.6%) at the 410-LVL is sufficient to account for the magnitude of velocity anomalies in the upper mantle in the S-tomogram below. Regions "i" and "ii" indicate high velocity regions that are either slab fragments or lithospheric delamination. Note that the region of the 410 near (ii) does not contain a 410-LVL.
The region labeled "3" in the S-tomogram roughly corresponds to the negative polarity 530-km arrival found in the Global Waveform Stack (Section 3).

6. Summary & Outlook

1. A 410 Low-Velocity Layer has been characterized beneath the LA RISTRA Array. The 410-LVL is 32.5 km thick with sharp top gradient and diffuse bottom gradient, and contains a 4.6% shear wave velocity reduction.

2. The 410-LVL is *not* detected in the SE portion of the study area, a region previously interpreted to be undergoing lithospheric delamination. A future study will examine the 410-km discontinuity to the NW of the LA RISTRA Array using RISTRA 1.5 data. Preliminary results are shown in the gray box.

3. A negative polarity P530s arrival has been identified. This arrival may be a manifestation of an intermittent "reverse" water-filter process within the transition zone.

4. Low velocity anomalies in the upper mantle may be caused by buoyant upwelling of hyrdous melt-diapirs from the 410-LVL.

The hypothesis drawn above in (4) is testable by surface wave tomography made possible by the Earthscope Transportable Array.

Summary of the transition zone water filter model (Bercovici & Karato, 2003). Hydrated wadsleyite fluxing through the olivine-wadsleyite phase loop crosses the wet solidus resulting in partial melt. The melt contains incompatible elements, e.g. U, Th. The altered upwelling material becomes MORB source obviating the need for a pre-existing MORB type chemical reservoir in the upper mantle.

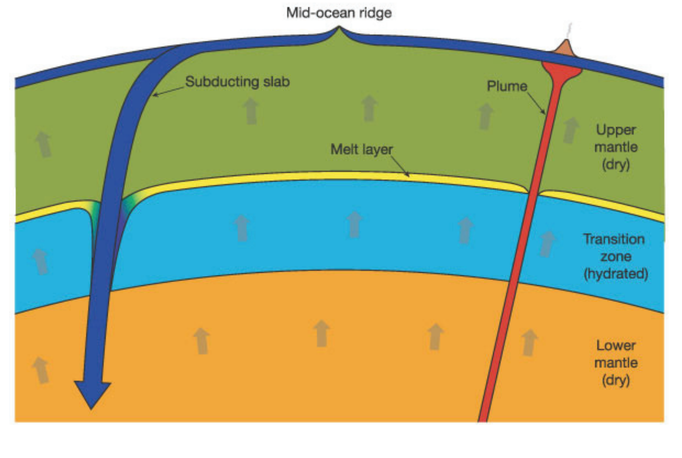

Bercovici & Karato 2003. Water-filter model summary.